Estimate low- and high-order wavefront using P1640 calibrator measurements

C. Zhai, G. Vasisht, M. Shao, T. Lockhart, E. Cady, et al.

C. Zhai, G. Vasisht, M. Shao, T. Lockhart, E. Cady, B. Oppenheimer, R. Burruss, J. Roberts, C. Beichman, D. Brenner, J. Crepp, R. Dekany, L. Hillenbrand, S. Hinkley, I. Parry, L. Pueyo, E. Rice, L. C. Roberts, A. Sivaramakrishnan, R. Soummer, H. Tang, F. Vescelus, K. Wallace, N. Zimmerman, "Estimate low- and high-order wavefront using P1640 calibrator measurements," Proc. SPIE 8864, Techniques and Instrumentation for Detection of Exoplanets VI, 88640L (26 September 2013); doi: 10.1117/12.2024754

SPIE.

Event: SPIE Optical Engineering + Applications, 2013, San Diego, California, United States

Estimate low and high order wavefront using P1640 Calibrator measurements

C. Zhai *[a], G. Vasisht [a], M. Shao [a], T. Lockhart [a], E. Cady [a], B. Oppenheimer[b], R. Burruss[a], J. Roberts [a], C. Beichman[c], D. Brenner[b], J. Crepp[d], R. Dekany[c], L. Hillenbrand[c], S. Hinkley[c], I. Parry[e], L. Pueyo[f], E. Rice[b], L. C. Roberts Jr. [a], A. Sivaramakrishnan[g], R. Soummer[f], H. Tang[a], F. Vescelus[a], K. Wallace [a], N. Zimmerman[h]

[a]Jet Propulsion Laboratory, California Institute of Technology, 4800 Oak Grove Dr, Pasadena, CA, 91109; [b]Dept. American Museum of Natural History, Central Park West at 79th Street, New York, NY 10024; [c]California Institute of Technology, 1200 E. California Blvd., Pasadena, CA 91125; [d]University of Notre Dame, IN 46556; [e]Institute of Astronomy, Cambridge University; [f]Johns Hopkins University, Physics and Astronomy Dept., Baltimore, MD 21218 USA; [g]Space Telescope Science Institute, Baltimore, MD 21218, USA; [h]Max Planck Institute for Astronomy, Heidelberg, Germany; Department of Physics,

ABSTRACT

P1640 high contrast imaging system on the Palomar 200 inch Telescope consists of an apodized-pupil Lyot coronagraph, the PALM-3000 adaptive optics (P3K-AO), and P1640 Calibrator (CAL). Science images are recorded by an integral field spectrograph covering J-H bands for detecting and characterizing stellar companions. With aberrations from atmosphere corrected by the P3K-AO, instrument performance is limited mainly by the quasi-static speckles due to non-common path wavefront aberrations for the light to propagate to the P3K-AO wavefront sensor and to the coronagraph mask. The non-common path wavefront aberrations are sensed by CAL, which measures the post-coronagraph E-field using interferometry, and can be effectively corrected by offsetting the P3K-AO deformable mirror target position accordingly. Previously, we have demonstrated using CAL measurements to correct high order wavefront aberrations, which is directly connected to the static speckles in the image plane. Low order wavefront, on the other hand, usually of larger amplitudes, causes light to leak through the coronagraph making the whole image plane brighter. Knowledge error in low order wavefront aberrations can also affect the estimation of the high order wavefront. Even though, CAL is designed to sense efficiently high order wavefront aberrations, the low order wavefront front can be inferred with less sensitivity. Here, we describe our method for estimating both low and high order wavefront aberrations using CAL measurements by propagating the post-coronagraph E-field to a pupil before the coronagraph. We present the results from applying this method to both simulated and experiment data.
Keywords: wavefront, estimation, low order, coronagraph, calibrator

1. INTRODUCTION

P1640 high contrast imaging system on the Palomar 200 inch Telescope is effective for detecting and characterizing stellar companions covering J-H spectral bands [1]. It consists of the P1640 apodized-pupil Lyot coronagraph with an integral field spectrograph, the PALM-3000 adaptive optics (P3K-AO), and the P1640 Calibrator (CAL)[2]. While the P3K-AO system effectively removes wavefront aberrations due to atmosphere, the quasi-static speckles due to the non-common path wavefront errors limits the contrast ratio. The non-common path wavefront errors come from the different optical paths taken by the light to propagate from the deformable mirror (DM) to the AO wavefront sensor and to the coronagraph focal plane mask. To achieve the highest contrast, the most important wavefront is at just before the focal plane mask of the coronagraph, where most of the star light (within a hole of diameter $5.2\lambda/D$) is rejected. Even though the wavefront at the AO wavefront sensor is well corrected by DM, the wavefront at just before the focal plane mask may still contains aberrations due to the non-common path error. To sense the non-common path wavefront error, P1640 calibrator measures the post-coronagraph wavefront using interferometry, by interfering the post-coronagraph light (science beam) before going to the Lyot stop with a reference beam formed by low-pass filtering the blocked star light at the coronagraph focal plane mask using a pinhole of diameter $1.4\lambda/D$. See Figure 1 for a sketch.

Techniques and Instrumentation for Detection of Exoplanets VI, edited by Stuart Shaklan, Proc. of SPIE
Vol. 8864, 88640L · © 2013 SPIE · CCC code: 0277-786X/13/$18 · doi: 10.1117/12.2024754

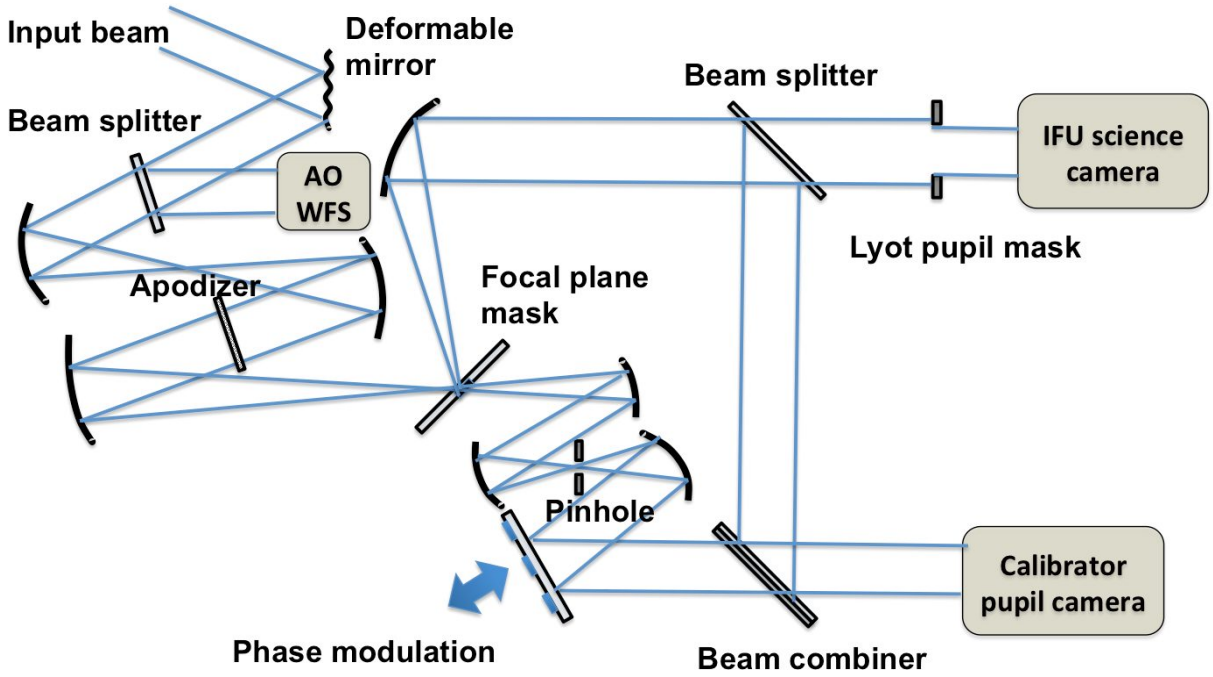

Figure 1, Schematic diagram of P1640 high contrast imaging system, which includes P1640 coronagraph, Pal3000 AO system, and the P1640 Calibrator.

By design, the coronagraph optimally suppresses the starlight with an ideal wavefront. Any deviations from an ideal wavefront increase the light leaking through the coronagraph and thus degrade the contrast ratio. This allows a post-coronagraph wavefront sensor like CAL to sense the wavefront of the input beam to the coronagraph. Because the focal plane mask radius is $\rho\lambda/D$, $\rho = 2.6$, wavefront errors with spatial frequencies higher than $2.6/D$ can go through the coronagraph efficiently. By sensing the post-coronagraph E-field, P1640 calibrator senses effectively the wavefront errors of spatial frequency higher than $2.6/D$ in the input beam before the coronagraph. This enables us to correct the wavefront errors in the input beam using the DM, and thus improve the imaging quality as demonstrated in a previous work [3]. The low order wavefront error at the input beam, however, is attenuated by the coronagraph before being measured by CAL. Therefore CAL senses low order wavefront aberrations in the input beam less efficiently. Because the non-common path wavefront errors are quasi-static at time scale of minutes, it is possible to use CAL to provide estimation of both low and high order wavefront aberrations in the input beam to generate DM correction to improve both low and order wavefront. This paper describes how to use the CAL measurement to estimate both low and high order wavefront aberrations at an input pupil (at DM) before the coronagraph. We also quantify the spatial frequency dependency in the CAL sensitivity using simulations. We found that the largest degradation in the sensitivity for estimating low order wavefront is approximately a factor of 5.

In a previous work, we presented a first order calibration and estimation algorithm using CAL measurement, focusing on estimating wavefront aberrations of high spatial frequencies [2]. There, we rely on a regular grid poking of high spatial frequency to calibration the low order phase that enables to estimate aberrations of high spatial frequency. We demonstrated the efficacy of correcting higher order wavefront aberrations using DM and thus reducing the speckles due to high order non-common path error. The drawback is that a new grid poking calibration is needed aach time when the low order wavefront changes in the input beam. Our current approach estimates the differential phase of the reference beam relative to the science beam, which is insensitive to the input wavefront. Therefore, this approach estimates simultaneously the low and high order wavefront and allows correcting low order wavefront without requiring extra calibration data allowing continuously improvement of the wavefront.

In the next section, we first describe measurements that can be taken by P1640 Calibrator and providing the basic mathematical relations for the wavefront estimation algorithm, which is subsequently presented. In section 3, we show results from simulation and analyzing CAL data taken in laboratory. Finally, we conclude with remarks on future works.

2. MODELS AND ALGORITM DESCRIPTIONS

CAL directly measures light at a post-coronagraph pupil, whose deviation from an ideal post-coronagraph wavefront enables us to estimate a correction at the DM pupil to improve the performance of the coronagraph. In this section, we provide CAL measurement models that relate the CAL measurements with the post-coronagraph E-fields and the model relating the input wavefront at the DM to the post-coronagraph E-fields.

2.1 Measurement models for P1640 Calibrator

The P1640 Calibrator measures interference fringes as the reference beam is phase modulated using a four step staircase modulation profile with π/2 step. The standard four-bin ABCD algorithm yields the fringe phasors [3],

$$\Phi(x,y) \equiv \frac{1}{4}[\,(A-C)+i(B-D)] = E_{ref}^{*}(x,y)E_{sci}(x,y) \tag{1}$$

where A,B,C,D are the four consecutive CAL intensity measurements and the phasor is the product of the E-fields $E_{sci}(x,y)$ and $E_{ref}(x,y)$ from the science and the reference beams respectively. Figure 2 displays the phase modulation profile and the corresponding camera frames from CAL.

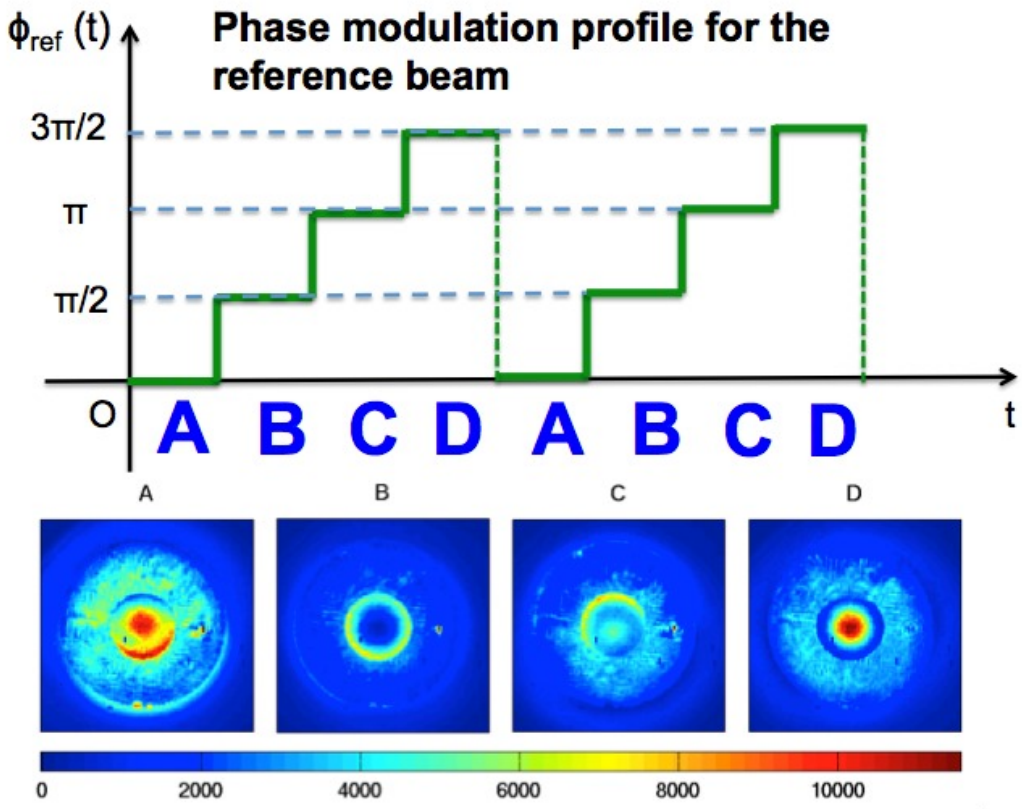

Figure 2, Phase modulation profile (top) and the corresponding P1640 Calibrator ABCD frames.

CAL is also capable to separately measure the intensities of the science and the reference beams at CAL pupil by using shutters. Figure 3 shows the intensities measured on P1640 CAL pupil for three cases: (a) reference beam only (b) science beam only, centered on coronagraph mask (c) science beam only, off from the center of coronagraph mask to form an un-occulted image of the input pupil.

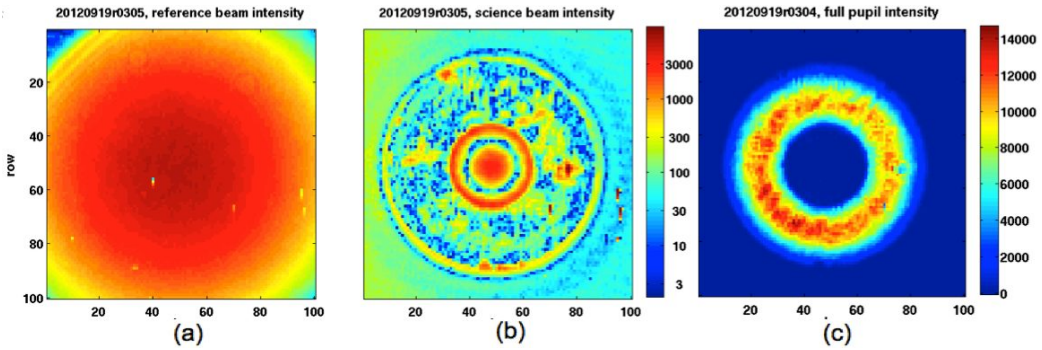

Figure 3, intensities of reference and science beams. (a) reference beam intensity (b) science beam intensity (c) science beam intensity when off the center of coronagraph mask, an un-occulted input pupil image.

The reference beam intensity $I_{ref}(x,y) \equiv \left|E_{ref}(x,y)\right|^2$, measured in case (a), can be used to parameterize the complex reference E-field as

$$E_{ref}(x,y) = \sqrt{I_{ref}(x,y)}\exp\{i\phi_{rs}(x,y)\}, \tag{2}$$

where $\phi_{rs}(x,y)$ is the low order differential phase between reference beam and the science beam. Because the reference beam is formed by low-pass filtering through a pinhole of diameter $1.4\lambda/D$, the reference E-field has a flat wavefront close to a plane wave with only very low order variation, which can be modeled as a combination of a few low order Zernike polynomials. The science beam intensity measured in case (b) can be used to determine the location of pupil. The fringe measurements ABCD frames are the interference between these two fields. The intensity measured in case (c), denoted as $I_{sci}^{un-occulted}(x,y)$ is obtained by steering the science beam away from the focal plane mask hole (nominally rejecting the star light). It is an image of the input pupil

$$I_{sci}^{un-occulted}(x,y) = |\, t_{sci}E_i(x,y)|^2, \tag{3}$$

where $E_i(x,y)$ represent the E-field at input pupil, which we shall use the DM pupil, and t_{sci} is a complex constant with $|t_{sci}|^2$ being the science arm throughput from the DM pupil to CAL camera pupil. This measurement will be used to constraint the input E-field amplitude.

2.2 Algorithm description

CAL measurements enable to estimate the post-coronagraph E-field, $E_{sci}(x,y)$ as

$$E_{sci}(x,y) = \frac{\Phi(x,y)}{E_{ref}^*(x,y)} = \Phi(x,y)/\sqrt{I_{ref}(x,y)}\exp\{\ i\ \phi_{rs}(x,y)\}. \tag{4}$$

Let the propagation of E-field from DM pupil to CAL camera pupil be the operator $\hat{T}_{sci}$ so that

$$E_{sci}(x,y) = \hat{T}_{sci}E_i(x,y). \tag{5}$$

Our algorithm for estimating the input wavefront at the DM pupil is based on inverting Eq. (5), to get $E_i(x,y) = T_{sci}^{-1}E_{sci}(x,y)$, and from $E_i(x,y)$ we can estimate both phase and amplitude.

However, since we need knowledge of $\phi_{rs}(x,y)$, it is useful to parameterize the differential phase $\phi_{rs}(x,y)$ using Zernike's polynomial,

$$\phi_{rs}(x,y) \approx \textstyle\sum_{l=1}^{n} C_l Z_l(x,y)\ , \tag{6}$$

where $Z_l(x,y)$'s are Zernike's polynomial and C_l's are coefficients. Because the reference beam is low-pass filtered by a pinhole, it is sufficient to use only use the first 5 Zernike's to cover up to quadratic phase terms. We estimate coefficients C_l's using the measured un-occulted pupil image intensity with the following minimization,

$$\min_{\{\alpha_m, C_l\}} \sum_{m=1}^{M} \left\{ \alpha_m \left| T_{sci}^{-1}\left[\frac{\Phi_m(x,y)\exp\left(\ i\sum_{l=1}^{n} C_l Z_l(x,y)\right)}{\sqrt{I_{ref}(x,y)}}\right]\right|^2 - I_{sci}^{un-occulted}(x,y)\right\}^2 \ , \tag{7}$$

where we allow to have multiple phasors $\Phi_m(x,y)$ to be used with m being the index and α_m's are fitting constants to account for any overall intensity fluctuations. Once C_l's are determined and so is the differential phase, the input E-field is then estimated as

$$E_i(x,y) = T_{sci}^{-1}\left[\frac{\Phi(x,y)\exp\left(i\sum_{l=1}^{n} C_l Z_l(x,y)\right)}{\sqrt{I_{ref}(x,y)}}\right]. \tag{8}$$

We summarize the data processing for the algorithms in the following flow charts shown in Figure 4, where the flow chart (a) describes the data processing for estimating the Zernike coefficients C_l's by constraining the magnitude of the E-field at the DM pupil from the inverse propagating the measured post-coronagraph E-fields. The constraint is imposed by the fitting described by Eq. (7). Flow chart (b) describes the estimation of the phase and amplitude from the inverse propagation of the post-coronagraph E-field.

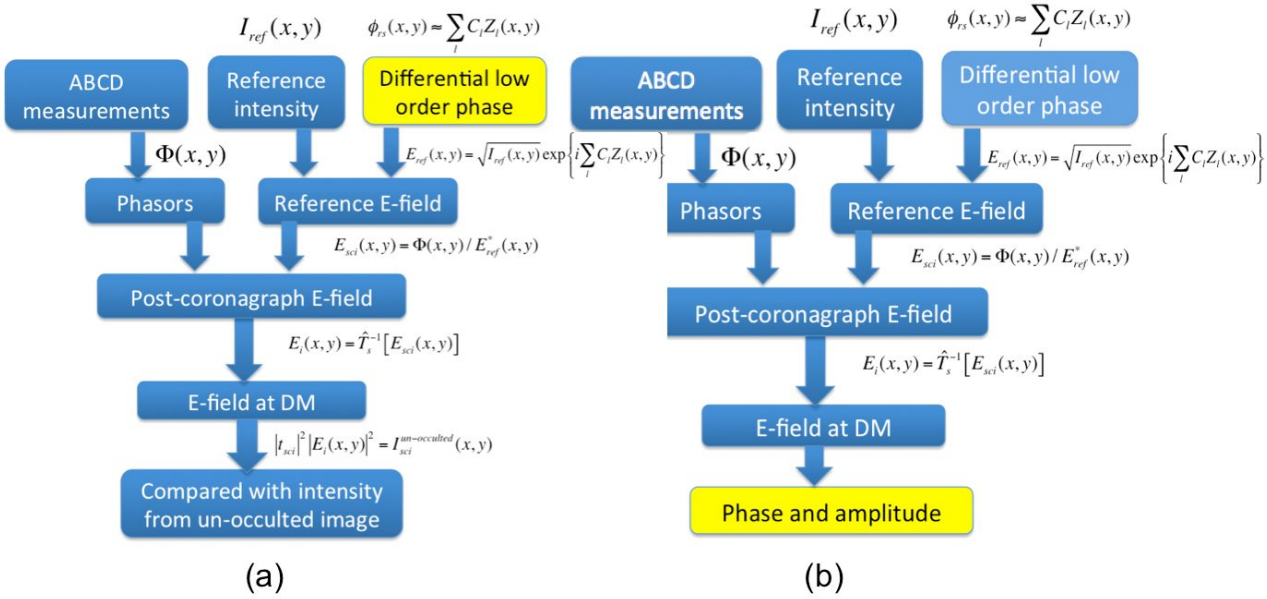

Figure 4, flow charts showing the data processing in the algorithms for estimating the reference beam phase relative to the science beam (a) and the wavefront at the DM pupil (b).

We note that the operator $\hat{T}_{sci}$ for propagation E-field at DM to CAL pupil does a high pass filtering. By Fourier optics, the operation of $\hat{T}_{sci}$propagation can be calculated following a standard integration for getting the Airy diffraction pattern:

$$E_{sci}(x,y) = \hat{T}_{sci}E_i(x,y) = t_{sci}\left[E_i(x,y) - \rho\int dx'\int dy' \frac{J_1\left(\frac{\rho\sqrt{\{x-x'\}^2+(y-y')^2}}{D}\right)}{\sqrt{\{x-x'\}^2+(y-y')^2 D}} E_i(x',y')\right], \tag{9}$$

where $\rho = 2.6$ is the radius of the coronagraph focal plane mask. By design, T_{sci} attenuates the E-field corresponding to an ideal wavefront the most, which we call it the 1st mode. Therefore, when we take the inverse of T_{sci}, we first project out the 1st mode of T_{sci} to avoid close to singular behavior. For other low order modes, T_{sci} does not attenuate as much (no more than a factor of 5). Bu the inverse T_{sci}^{-1} does amplify low order errors as we shall see in the sensitivity study results.

3. RESULTS

In this section, we present results from applying the algorithms described in the previous section to simulated data and P1640 data in laboratory.

3.1 Results based on Simulations

We simulate the P1640 Calibrator measurements based on the configuration parameters of P1640 imaging system to study the performance of wavefront estimation. Random phase aberrations with RMS~0.7rad~180nm and $1/f^3$ power spectrum are used. A 1% level Gaussian random white noise is added separately to real and imaginary parts of the phasors to simulate random error in its measurements. This is the level comparable with that of one set of P1640 CAL ABCD measurements in lab. Figure 5 shows one typical low order differential phase $\phi_{rs}(x, y)$ in the reference beam E-field with RMS ~ 180nm (a) and the estimated error in the differential phase is a few nanometers.

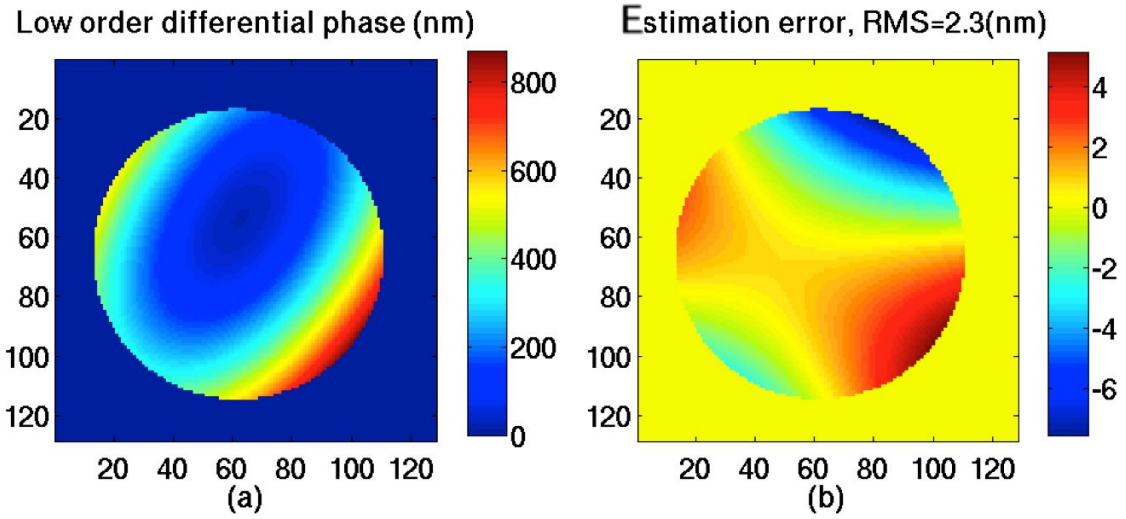

Figure 5, low order differential wavefront, and estimation error from simulation

Figure 6 shows the RMS of the estimation errors from 100 Monte Carlo runs with average value of 4.3nm.

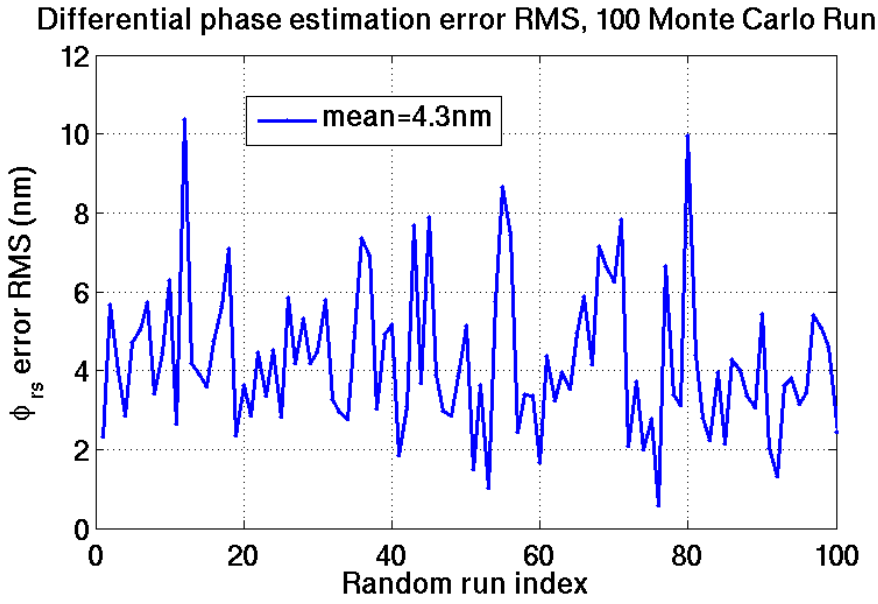

Figure 6, differential phase in reference beam estimation error statistics from 100 Monte Carlo runs.

Figure 7 shows an example of the wavefront phase aberration (a) used in the study with RMS 180nm and the estimation error (b) with RMS 6.1nm. The phase aberration (a) pattern is dominated by low order feature because it is generated randomly by using $1/f^3$ power spectrum. The estimation error (b) is almost white but with some extra low order feature which is due to the amplification of error in the estimation data processing or the degraded sensitivity. Figure 8 displays the error RMSs in estimating the input phase aberrations from 100 Monte Carlo runs. We found that the average estimation error is 6.1nm.

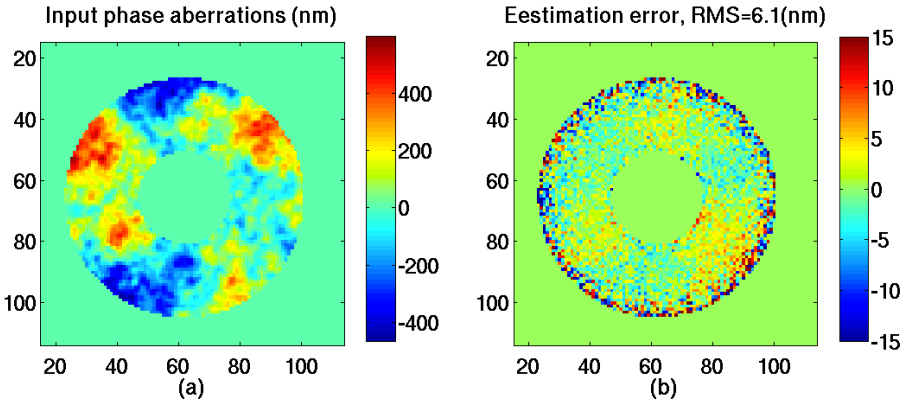

Figure 7, wavefront aberration at the DM pupil (a), RMS~180nm, and estimation error using CAL measurements

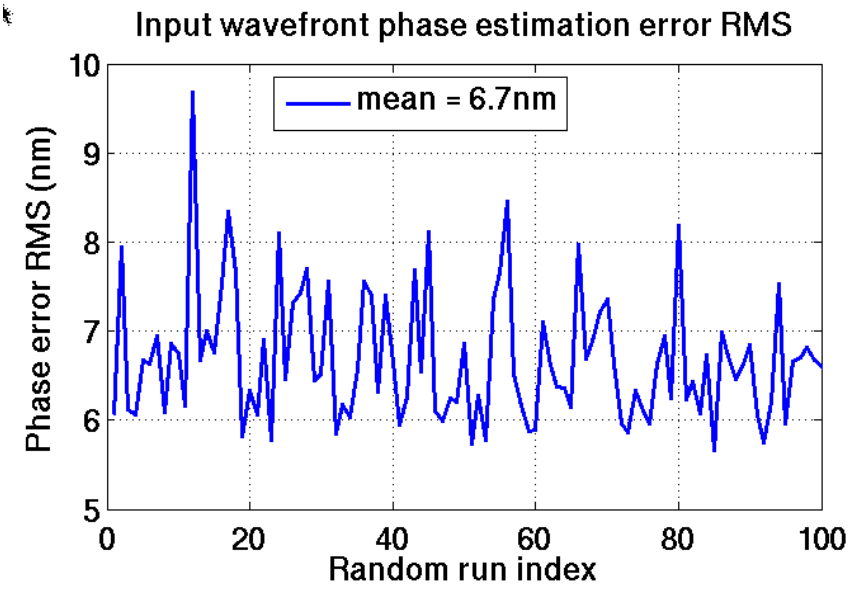

Figure 8, RMS of input phase estimation errors at DM pupil from 100 Monte Carlo runs.

We performed a spatial spectral analysis of the phase estimation error and display the normalized spectrum in Figure 9. Because we added white noises as the measurement errors, we expect error to be white if the sensitivity to error is independent of the spatial frequency. According to Figure 9, the error has much larger amplitude in lower spatial frequencies, especially when it is lower than 3/D. This shows that the sensitivity is poor due to the high pass filtering effect of the coronagraph as expected. We see that the worst degradation of sensitivity is approximately a factor of 5.

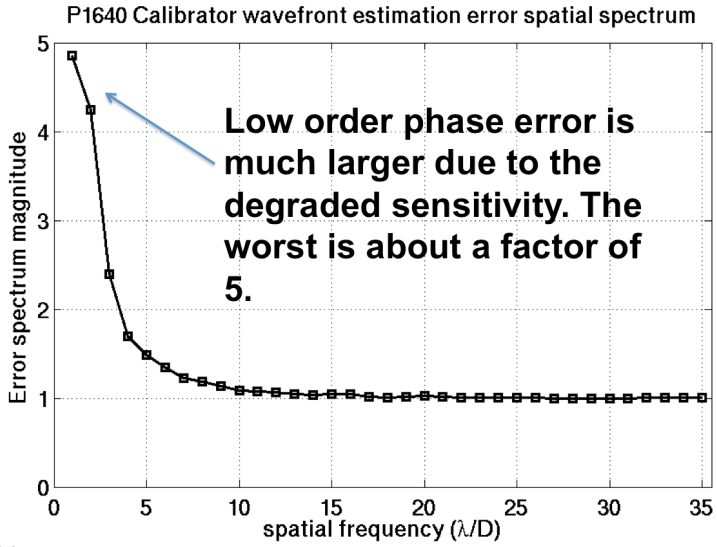

Figure 9. P1640 Calibrator sensitivity as function of spatial frequency, normalized to 1 at high spatial frequency.

3.2 Results using P1640 data taken in laboratory

We applied the wavefront estimation algorithm to P1640 CAL data taken in lab using internal source on Dec 23, 2012. Correction command is generated according to the estimated wavefront and sent to DM to improve the wavefront using a gain of 0.25. Figure 10 shows the estimated wavefront maps during the four DM correction iterations. There are some improvements, but it converges much slower than what we expected. It is part of our future work to understand this.

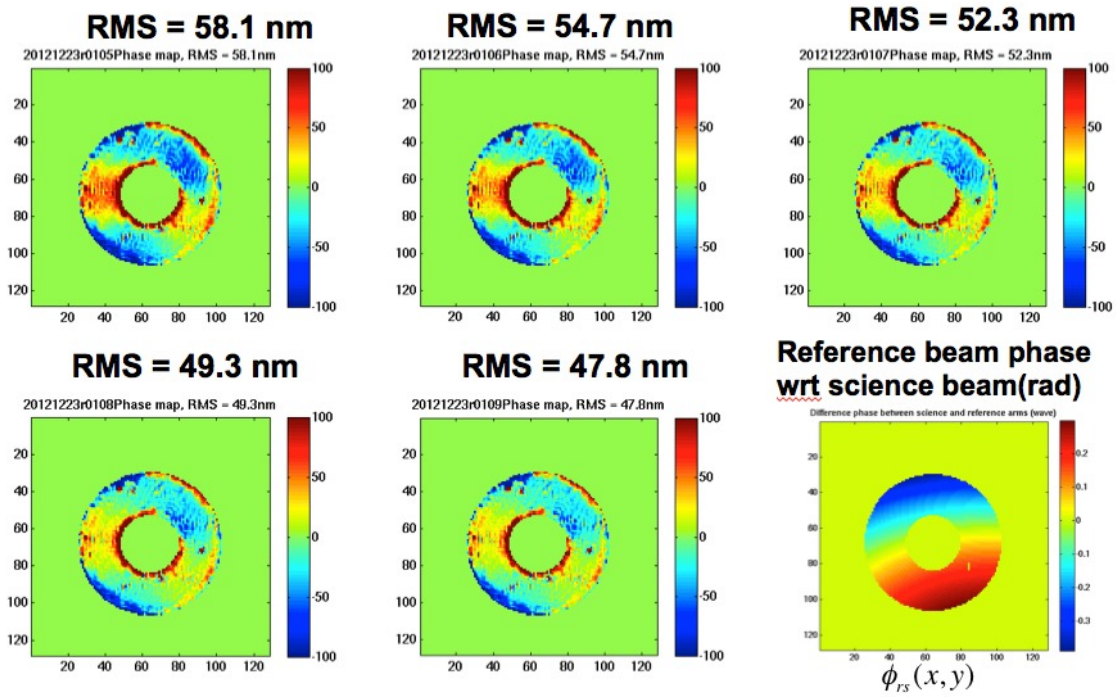

Figure 10, estimated input wavefront phase maps before and after four iterative DM corrections in order : upper left, mid, right, and then lower left and mid. The last phase map is the low order phase of reference beam relative to the science beam.

4. CONCLUSIONS AND FUTURE WORKS

We have presented an algorithm that can estimate input wavefront aberrations of both low and high spatial frequencies using the P1640 CAL measurements. By taking the un-occulted pupil image on CAL camera, it is possible to solve for the low order differential phase in the reference beaachievm relative to the science beam. For typical noise level of P1640 CAL using internal light source in lab, we expect the wavefront estimation error RMS to be less than 10nm. Because CAL senses post-coronagraph E-field, its sensitivity to low order wavefront aberrations in the input beam is degraded by the coronagraph focal plane mask. Sensitivity study shows the largest degradation in sensitivity are for the low frequency modes and no worse than a factor of 5. Applying the algorithm to P1640 CAL lab data, we were able to improve the wavefront by DM correction based on commands generated by the estimated wavefront. This approach enables to continuously improve wavefront without additional calibration.

Future works include studying the sensitivity of the algorithm to the knowledge of the location of pupil and size and the size of the focal plane mask, exploring techniques for improving sensitivity to low order wavefront by incorporating additional calibration data, and conducting more analysis of lab data to understand the reason why the low order correction to does not perform as expected.

ACKNOWLEDGEMENTS

This work was prepared at the Jet Propulsion Laboratory, California Institute of Technology, under a contract with the National Aeronautics and Space Administration.

REFERENCES

[1] B. R. Oppenheimer, C. Baranec, C. Beichman, D. Brenner, R. Burruss, E. Cady, J. R. Crepp, R. Dekany, R. Fergus, D. Hale, L. Hillenbrand, S. Hinkley, David W. Hogg, D. King, E. R. Ligon, T. Lockhart, R. Nilsson, I. R. Parry, L. Pueyo, E. Rice, J. E. Roberts, L. C. Roberts, Jr., M. Shao, A. Sivaramakrishnan, R. Soummer, T. Truong, G. Vasisht, A. Veicht, F. Vescelus, J. K. Wallace, C. Zhai, and N. Zimmerman1, *Reconnaissance of the HR8799 Exosolar System I: Near IR Spectroscopy*, ApJ, **768**, 24, (2013).

[2] Hinkley, S.; Oppenheimer, B. R.; Zimmerman, N.; Brenner, D.; Parry, I. R.; Crepp, J. R.; Vasisht, G.; Ligon, E.; King, D.; Soummer, R.; Sivaramakrishnan, A.; Beichman, C.; Shao, M.; Roberts, L. C.; Bouchez, A.; Dekany, R.; Pueyo, L.; Roberts, J. E.; Lockhart, T.; Zhai, C.; Shelton, C.; Burruss, R., "New High Contrast Imaging Program at Palomar Observatory, " Publications of the Astronomical Society of the Pacific, Volume 123, p.74-86, doi: 10.1086/658163, (2011).

[3] C. Zhai, G. Vasisht, M. Shao, T. Lockhart, E. Cady, B. Oppenheimer, R. Burruss, J. Roberts, C. Beichman, D. Brenner, J. Crepp, R. Dekany, S. Hinkley, L. Hillenbrand, E. R. Ligon, I. Parry, L. Pueyo, E. Rice, L. C. Roberts, A. Sivaramakrishnan, R. Soummer, F. Vescelus, K. Wallace, N. Zimmerman, "A first order wavefront estimation algorithm for P1640 calibrator," Proc. SPIE 8447, Adaptive Optics Systems III, 84476W, doi:10.1117/12.927015 (2012).